

RESEARCH

Open Access



FSTL1 accelerates nucleus pulposus-derived mesenchymal stem cell apoptosis in intervertebral disc degeneration by activating TGF- β -mediated Smad2/3 phosphorylation

Xu Yan^{1,2,3}, Jing-Yu Ding^{1,2,3}, Ren-Jie Zhang^{1,2,3}, Yan-Xin Wang^{1,2,3}, Lu-Ping Zhou^{1,2,3}, Hua-Qing Zhang^{1,2,3}, Liang Kang^{1,2,3}, Chong-Yu Jia^{1,2,3}, Xiao-Ying Liu^{4*} and Cai-Liang Shen^{1,2,3*} 

Abstract

Background Intervertebral disc degeneration (IVDD) is the leading cause of low back pain, and repair using nucleus pulposus-derived mesenchymal stem cells (NP-MSCs) represents a promising therapeutic approach. However, both endogenous and transplanted NP-MSCs demonstrate limited proliferative capacity, increased apoptosis, and reduced resilience to the harsh microenvironment within the degenerative intervertebral disc (IVD).

Methods RNA sequencing (RNA-seq) was utilized to identify genes and associated mechanisms that mediate the responses of NP-MSCs to acidic conditions. Western blotting, qPCR, and immunofluorescence were used to evaluate follistatin-like 1 (FSTL1) expression in NP-MSCs. Apoptosis and extracellular matrix (ECM) anabolism were assessed via flow cytometry, TUNEL staining and Western blotting, while the TGF- β /Smad2/3 pathway was analyzed using Western blotting and immunofluorescence. FSTL1 knockdown with small interfering RNA (siRNA) was performed to determine its role in apoptosis and ECM regulation. The FSTL1 siRNA pretreatment was assessed in a puncture-induced rat IVDD model using MRI and histological staining.

Results Using RNA-seq, we identified FSTL1 as the primary acid-responsive gene in NP-MSCs. We further observed elevated FSTL1 expression in NP-MSCs isolated from degenerative IVDs in both humans and rats compared to normal IVDs. Acidic conditions upregulated FSTL1 expression in NP-MSCs in a pH-dependent manner. Notably, recombinant FSTL1 was shown to enhance cellular apoptosis and disrupt ECM metabolism. Conversely, silencing FSTL1 with siRNA reduced NP-MSC apoptosis and improved ECM anabolism. Importantly, TGF- β pathway inhibition partially reversed the pro-apoptotic and ECM catabolism effects of FSTL1. In the rat model of IVDD, pretreatment of NP-MSCs with FSTL1 siRNA significantly suppressed IVDD progression.

*Correspondence:

Xiao-Ying Liu
liuxiaoying@ahmu.edu.cn
Cai-Liang Shen
shencailiang@ahmu.edu.cn

Full list of author information is available at the end of the article



© The Author(s) 2025. **Open Access** This article is licensed under a Creative Commons Attribution-NonCommercial-NoDerivatives 4.0 International License, which permits any non-commercial use, sharing, distribution and reproduction in any medium or format, as long as you give appropriate credit to the original author(s) and the source, provide a link to the Creative Commons licence, and indicate if you modified the licensed material. You do not have permission under this licence to share adapted material derived from this article or parts of it. The images or other third party material in this article are included in the article's Creative Commons licence, unless indicated otherwise in a credit line to the material. If material is not included in the article's Creative Commons licence and your intended use is not permitted by statutory regulation or exceeds the permitted use, you will need to obtain permission directly from the copyright holder. To view a copy of this licence, visit <http://creativecommons.org/licenses/by-nc-nd/4.0/>.

Conclusions This study provides novel insights into the mechanistic role of FSTL1 in acid-induced apoptosis of NP-MSCs and its contribution to the progression of IVDD. These findings offer valuable perspectives for developing targeted therapeutic strategies to mitigate IVDD progression.

Keywords FSTL1, Cellular apoptosis, IVDD, TGF- β /Smad2/3

Introduction

Despite surgical and medical advancements, low back pain (LBP) continues to be a significant contributor to health expenditure and financial strain [1, 2]. The primary pathological cause of LBP has been identified as intervertebral disc degeneration (IVDD) [3], which has gained increasing attention in the field of regenerative medicine [4, 5]. The intervertebral disc (IVD) has been identified as an immune-exempt region [6], an enabling characteristic for using stem cells to treat IVDD [7]. Mesenchymal stem cells (MSCs), including those derived from adipose tissue, bone marrow, and umbilical cord, have become increasingly prevalent as the basis for IVDD treatment [8–11].

Compared to exogenous MSCs, nucleus pulposus-derived mesenchymal stem cells (NP-MSCs) found within the IVD have emerged as a promising seed cell resource. Notionally, NP-MSCs appear better adapted to the microenvironment of degenerative IVDs, making them a more suitable candidate for regenerative therapies [12]. Our previous research has validated the presence of NP-MSCs within degenerative nucleus pulposus (NP) tissues of humans [13, 14] while other research has shown these cells possess self-renewal and differentiation ability, giving rise to nucleus pulposus cells (NPCs) that are responsible for promoting anabolism of the extracellular matrix (ECM) [15]. Nonetheless, the harsh characteristics of the degenerative IVD microenvironment implicitly limits the ability of NP-MSCs to persist, ultimately resulting in the failure of stem cell-based IVD regeneration [16].

The IVD represents the biggest non-vascular tissue in the body [17]. The primary energy source is delivered through the capillaries of the IVD located in the vertebral bodies [18] which facilitate the diffusion of nutrients through the cartilage endplate (CEP) [19]. However, impairment of this process in IVDD allows metabolite accumulation, triggering an altered IVD microenvironment characterized by acidosis [20]. Our previous studies have demonstrated significant impacts of acidosis on NP-MSCs, inducing cellular senescence and apoptosis, followed by ECM degeneration and IVDD pathologies [13, 14]. Despite its importance, there has been limited research focusing on strategies to protect NP-MSCs from acid-induced cell death.

Follistatin-like 1 (FSTL1), initially identified as a transforming growth factor- β (TGF- β)-inducible gene, encodes a small glycoprotein belonging to the

cysteine-rich acidic protein family that is secreted into the ECM [21]. FSTL1 is widely expressed in all eukaryotic cells except for peripheral lymphocytes [22]. Previous studies link FSTL1 with the regulation of endocrine function, cell proliferation, apoptosis, metabolism, cell differentiation and immune responses [23–25] including a specific report where FSTL1 was demonstrated to regulate chondrocyte proliferation and promote MSC differentiation into chondrocytes [26]. Interestingly, high FSTL1 concentrations significantly inhibit MSC proliferation [27] while our previous study showed FSTL1 accelerated NPC senescence and ECM degeneration [28]. However, to date, the role of FSTL1 in NP-MSC degeneration and its molecular mechanisms contributing to IVDD remain unexplored.

Of further interest here is the TGF- β /Smad2/3 signaling pathway, a pivotal regulator of cellular processes such as differentiation, apoptosis, tissue fibrosis, and migration, is governed by TGF- β , a versatile cytokine that plays a crucial role in maintaining tissue homeostasis and orchestrating cellular responses to environmental stimuli [29, 30]. This pathway has been shown to significantly influence MSC behavior and play a critical role in the progression of IVDD [31, 32]. Notably, the FSTL1 protein, with its multi-functional domains-including a follistatin-like domain, Kazal-like domain, extracellular calcium-binding domain, Von Willebrand factor-type C domain, and signal peptide domain-interacts with components of the TGF- β superfamily to regulate chondrocyte proliferation, MSC differentiation, and ECM protein expression [33, 34]. Therefore, elucidating the role of FSTL1 within the TGF- β signaling network is essential to understanding its impact on NP-MSC degeneration and IVDD progression.

In this study, we hypothesized that FSTL1 accelerates NP-MSC apoptosis and ECM degeneration by activating the TGF- β /Smad2/3 signaling pathway. To test this, we utilized an acid-induced NP-MSC degeneration model *in vitro* and a rat puncture-induced IVDD model *in vivo*. We examined the effects of FSTL1 knockdown via small interfering RNA (siRNA) and its upregulation through recombinant FSTL1 (r-FSTL1) treatment on NP-MSC apoptosis and ECM degeneration. Additionally, we demonstrated that the TGF- β inhibitor SB-431542 effectively reduced NP-MSC apoptosis and ECM degradation. Together these findings suggest FSTL1 as a potential therapeutic target for IVD regeneration.

Materials and methods

Human NP tissues

NP tissues were obtained from patients undergoing surgery at the First Affiliated Hospital of Anhui Medical University for IVDD or vertebral fracture. Six mildly degenerated NP tissues were collected from 6 patients who underwent vertebral fracture while six severely degenerated NP tissues were collected from 6 IVDD patients. Prior to surgery, standard T2-weighted magnetic resonance imaging (MRI) examinations were conducted on the lumbar spine after which three impartial observers scored the degree of IVDD according to the Pfirrmann classification and MRI results (Table 1). After excision, NP tissues were divided into two for the purposes of histological staining and cell isolation. This study was approved by the Medical Ethics Committee of Anhui Medical University.

Rat IVDD model

Thirty Sprague-Dawley (SD) rats were randomly divided into six groups: (A) Control group: Received anesthesia but no IVD intervention. (B) IVDD group: Annulus fibrosus (AF)-punctured IVDs. (C) PBS group: Phosphate-buffered saline (PBS) injected into AF-punctured IVDs. (D) NP-MSc group: Normal rat NP-MSCs transplanted into AF-punctured IVDs. (E) NC siRNA group: Negative control siRNA (si-NC) pretreated NP-MSCs transplanted into AF-punctured IVDs (F) FSTL1 siRNA group: FSTL1 siRNA pretreated NP-MSCs transplanted into the AF-punctured IVDs. Transplanted cells were added twice a week (eight times in total) for groups D-E. AF punctures were performed as previously described [28]. Briefly, after anesthesia, rats were positioned prone before using a 21G needle to percutaneously puncture the caudal IVDs (C6/7). The needle was positioned at the center of the disc and introduced at a right angle to the skin and parallel to the endplate before 180 degrees rotation maintained for a duration of 5 s. MRI scans were performed at four weeks after the procedure. Studies were conducted

in accordance with the Laboratory Animal Center of Anhui Medical University's authorization and in accordance with the International Guiding Principles for Animal Research.

Histology

After paraffin embedding, 5 μ m sections of NP tissues were stained with Alcian blue, Safranin O-Fast Green (SO), or Hematoxylin-Eosin (H&E). The histological scores of IVDs were assessed in accordance with specified criteria by three impartial observers [35].

NP-MSc isolation and culture

Primary human NP-MSCs were isolated using the previously described method [14] while primary rat NP-MSCs were isolated from NP tissue of the caudal vertebrae of SD rats. Tissues were digested using type II collagenase solution (Sigma-Aldrich, USA) for 3-hours at 37 °C before subsequently culturing the residual microtissue and cells in low-glucose Dulbecco's modified Eagle's medium (HyClone, USA) supplemented with 10% fetal bovine serum (Gibco Life Technologies, UK) and a 1% penicillin-streptomycin at 37 °C in a humidified environment with 5% CO₂. The culture medium was replaced twice a week and once cultures reached 80–90% confluence, the cells were passaged at 1:3 a ratio. Subsequent experiments utilized cells at passage 3 (P3).

Surface marker identification

Suspensions of NP-MSc cultures at 1.5×10^6 cells/mL were prepared by trypsin digestion and resuspended in PBS. The cells were then subjected to immunophenotyping utilizing flow cytometry using fluorophore-conjugated monoclonal antibodies against CD45-PE, CD34-PE, HLA-DR-APC, CD73-FITC, CD90-FITC, and CD105-PE, or isotype controls (all obtained from eBioscience, USA). Following guidelines provided by the International Society for Cellular Therapy, the cells were incubated with antibodies at 25 °C for 30 min in the dark prior to twice washing with cold PBS and resuspension in 500 μ L of PBS containing 1% formaldehyde. The cells underwent examination by flow cytometry (Beckman, USA) following established protocols with analysis conducted on a minimum of three samples for each surface marker. The proportion of positively stained cells was determined in relation to the isotype control.

Transcriptome sequencing

Comparator groups for RNA-seq involved NP-MSCs cultures receiving fresh complete medium or pH 6.6 conditioned medium. After 24 h, the cell monolayers were washed three times with PBS, and lysed with 1 mL of RNAiso lysis. The solution was removed and subjected to repeated vortexing before subsequent storage

Table 1 Patient demographic data and degree of IVDD

Case No	Gender	Pfirrmann grade
Case 1	Male	I
Case 2	Female	I
Case 3	Male	II
Case 4	Male	II
Case 5	Female	II
Case 6	Female	II
Case 7	Female	IV
Case 8	Female	IV
Case 9	Male	IV
Case 10	Female	V
Case 11	Male	V
Case 12	Male	V

at -80°C . for a prolonged period of time. RNA-seq and subsequent analyses were performed by Lianchuan Biology company.

Western blotting

Extraction of total protein was performed as described previously [28]. Primary antibodies used included: FSTL1 (1: 1000, ab223287, Abcam), MMP3 (1: 1000, ab52915, Abcam), MMP13 (1: 1000, ab39012, Abcam), Collagen II (1: 1000, ab34712, Abcam), Aggrecan (1: 1000, ab3778, Abcam), cleaved Caspase-3 (1: 1000, ab32042, Abcam), Bcl-2 (1: 1000, ab32124, Abcam), Bax (1: 1000, ab32503, Abcam), Smad2 (1: 1000, 5339 S, Cell Signaling Technology), p-Smad2 (1: 1000, 18338 S, Cell Signaling Technology), Smad3 (1: 1000, 9523 S, Cell Signaling Technology), and p-Smad3 (1: 1000, 9520 S, Cell Signaling Technology). The measurement of the integrated density of each blotting was conducted using ImageJ software, with loading normalization applied to the β -actin control.

qPCR

Total RNA extraction and reverse transcription were performed as described previously [35]. The qPCR experiments were conducted on an ABI Real-Time PCR System (Thermo Fisher Scientific, USA) with the indicated primers (Table 2). Cycle threshold (Ct) values were normalized to β -actin, and the $2^{-\Delta\Delta\text{Ct}}$ method was employed to compute comparative expression values.

Immunofluorescence staining

NP-MSCs cultivated on glass coverslips were subjected to fixation in 4% formaldehyde solution for 15 min before subsequent permeabilization using 0.1% Triton X-100 solution in PBS for 10 min and blocking with 5% bovine serum albumin (BSA) for 30 min. Thereafter, samples were incubated at 4°C overnight with primary antibodies: FSTL1 (1: 200, ab223287, Abcam), Smad2 (1: 500, 5339 S, Cell Signaling Technology) and Smad3 (1: 500, 9523 S, Cell Signaling Technology), and the next day incubated with secondary antibodies for 1 h at room

temperature. After DAPI counterstaining, the coverslips were mounted on slides and imaged using an epifluorescence microscope.

TUNEL staining

A TUNEL staining kit (Beyotime, China) was employed to quantify DNA fragmentation, a hallmark of late-stage apoptosis. NP-MSCs cultures treated as indicated were subject to fixation using 4% formaldehyde at 25°C for 15 min, permeabilization with 0.1% Triton X-100 solution for 10 min followed by three washes with PBS. After the addition of TUNEL reagents and nuclear counterstaining with DAPI, the percentage of TUNEL positive cells was determined using a fluorescence microscope (Zeiss, Germany).

Flow cytometry

Apoptosis rates of NP-MSC cultures were determined using the Annexin V-FITC/PI apoptosis detection kit (Bestbio, China) according to the manufacturer's instructions. Briefly, cell suspensions prepared by trypsin digestion under EDTA free conditions were washed twice with PBS before resuspension in $400\ \mu\text{L}$ $1\times$ Annexin V of binding solution at approximately 1×10^6 cells/mL. Thereafter, $5\ \mu\text{L}$ Annexin V-EGFP staining solution was added and the cell suspension mixed and incubated for 15 min at 4°C . Finally, after adding $5\ \mu\text{L}$ PI staining solution, cell suspensions were mixed and incubated at 4°C for 5 min. Annexin and PI positivity was determined by flow cytometry (Beckman, USA) and the results expressed as early-apoptotic cells (Annexin V^+ /PI $^-$) and late-apoptotic cells (Annexin V^+ /PI $^+$).

Cell transfection

NP-MSCs were transiently transfected with negative control siRNAs and siRNAs targeting FSTL1 (Sigma Aldrich) at a concentration of 50 nM using Lipofectamine 3000, following the manufacturer's instructions.

Statistical analysis

Analyses were conducted using GraphPad Prism (V.8.0, GraphPad Software) with a minimum of three replicates for each experimental condition. The Kolmogorov-Smirnov test was employed to evaluate normality, whereas parameters that followed a normal distribution were examined using Student's t-test and one-way ANOVA with Tukey's post hoc test. Histological score analysis was conducted using the Kruskal-Wallis H test. Data are displayed as the mean value \pm standard deviation (SD) derived from separate experiments with p values below 0.05 deemed statistically significant.

Table 2 Primers used in RT-qPCR

	Gene	forward primer (5'-3')	reverse primer (5'-3')
For rat	FSTL1	AACAGCCATCAACATCACCACCTTAT	TTTCAGT-CAGCGTTCT-CATCA
	β -actin	ATCATTGCTCCTCCTGAGCG	AGCTCAGTAA-CAGTCCGCC
For human	FSTL1	GCCATGACCTGTGACGGAAA	CAGCGCT-GAAGTG-GAGAAGA
	β -actin	CGTTGACATCCGTAAGACCTC	TAGGAGC-CAGGGCAGT AATCT

Results

Transcriptome sequencing analysis to identify degeneration-associated genes in NP-MSCs

To better understand the mechanisms underlying the effects of acidification on NP-MSCs, we conducted transcriptome sequencing on NP-MSCs cultivated under pH 6.6 conditions, a physiologically-relevant level of acidification chosen from our previous studies [14]. We identified a total of 670 differentially expressed genes (DEGs) in NP-MSCs between the control (nondegenerative) and pH 6.6 (degenerative) conditions including 372 upregulated and 298 downregulated genes, respectively with the top 50 DEGs shown in the accompanying heatmap (Fig. 1A, B). DEGs with $|\log_2FC| \geq 0.75$ changes were uploaded to

Metascape with analysis identifying enriched pathways or related functions with q values < 0.05 , including the TGF- β pathway and ECM organization (Fig. 1C). Notably, based on our previous work [28] the occurrence of FSTL1 among the top 25 upregulated DEGs piqued our interest, along with the point that FSTL1 is known to interact with TGF- β -related pathway related proteins (Fig. 1D). This prompted us to further explore the function of FSTL1 in NP-MSCs and its relationship with the TGF- β pathway in IVDD related processes.

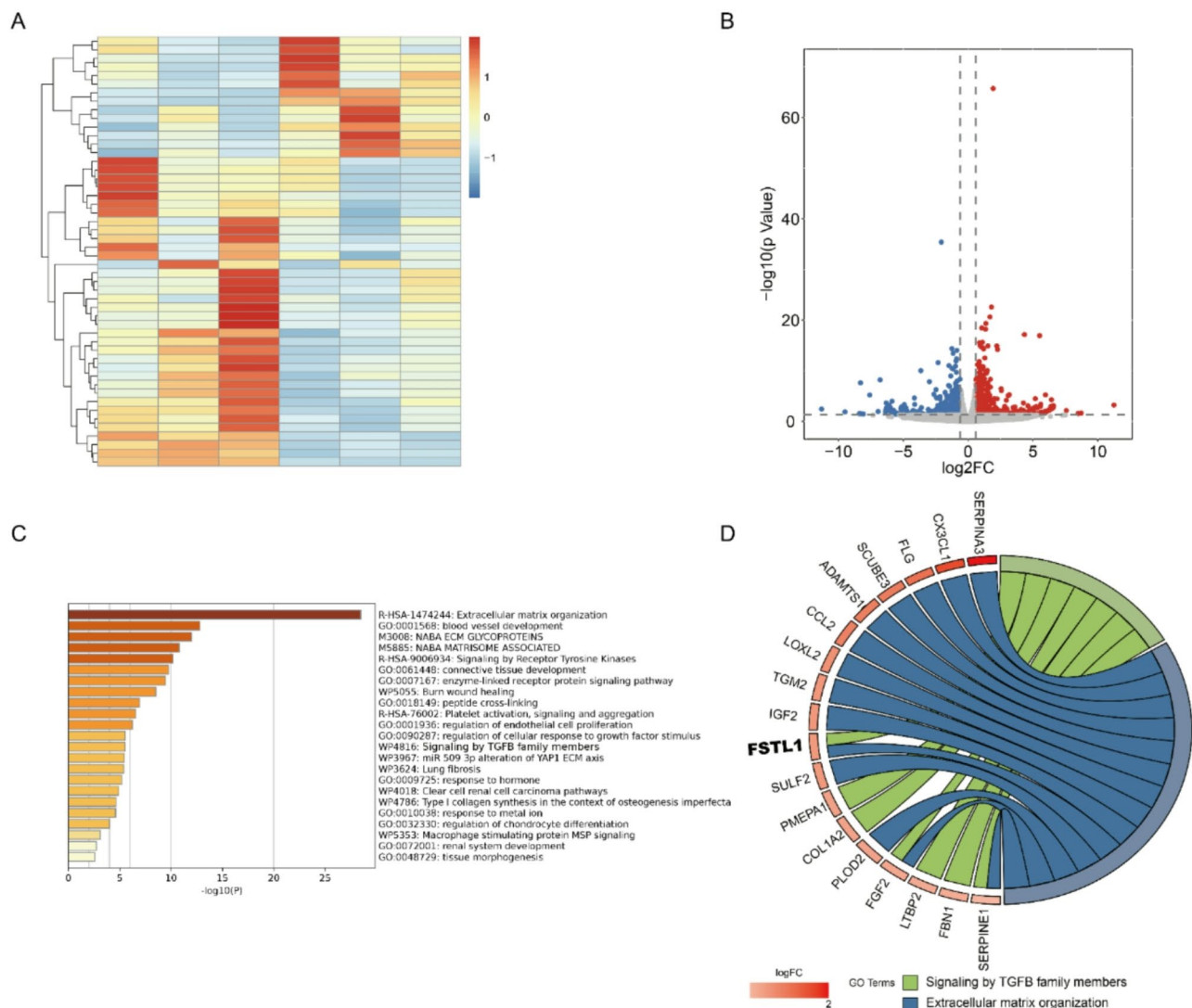


Fig. 1 Transcriptome sequencing reveals genes and pathways in NP-MSCs associated with acidic conditions. **(A)** Heatmap depicting hierarchical clustering of the top 50 downregulated and upregulated DEGs detected comparing NP-MSCs cultivated at pH6.6 and normal culture conditions using RNA-seq. Three biological replicates were used. **(B)** Volcano plot depicting significantly downregulated and upregulated DEGs. **(C)** Horizontal bar chart shows the top associated GO terms enriched against the DEGs ranked by p-values. **(D)** Circos plot showing differentially expressed genes. The left column represents differentially expressed genes, and the right column is different biological processes

FSTL1 expression increases in human NP-MSCs following degeneration

We first characterized NP tissues collected from patients with varying Pfirrmann grades. As expected, we found that severely degenerated NP tissues showed atrophic volume and decreased elasticity in comparison to mildly degenerated NP tissues (Fig. 2A). Moreover, H&E and Alcian blue staining showed that the number of NPCs and the proteoglycan content in the severely degenerated NP tissues were significantly reduced (Fig. 2B).

Next, we examined the expression status of FSTL1 protein in the NP-MSCs isolated from the severe and mildly degenerated NP tissues. Using Western blotting we observed that the expression of FSTL1 was considerably upregulated in NP-MSCs derived from severely degenerated NP tissues (Fig. 2C-D). Moreover, qPCR results corroborated that FSTL1 mRNA levels were much higher in severely degenerated NP-MSCs compared to mildly degenerated NP-MSCs (Fig. 2G). Furthermore, the results of immunofluorescence staining assays revealed a higher prevalence of FSTL1-positive cells in severely degenerated NP-MSCs (Fig. 2E-F). Thus, FSTL1

expression is positively associated with the degree of degeneration in NP-MSCs.

FSTL1 expression is upregulated in degenerated rat NP-MSCs

Given the physiological similarities between degenerated human and rat intervertebral discs, as well as the widespread use of rat models in IVDD research, we aimed to confirm whether FSTL1 expression is also elevated in NP-MSCs derived from a rat model of IVDD. Initial characterization of the control and IVDD group animals using T2-weighted MRI findings showed that AF puncture elicited significantly higher Pfirrmann grades (Fig. 3A-B). Further histological staining using H&E, SO and Alcian blue showed decreased NPCs with disordered NP morphology and AF with broken inner fibers and unclear boundary in AF puncture IVDs (Fig. 3C-D), together confirming the successful establishment of the rat IVDD model.

Thereafter, cells isolated and cultured from rat caudal IVDs were subject to verification by flow cytometry. This analysis showed the cultured cells were positive for

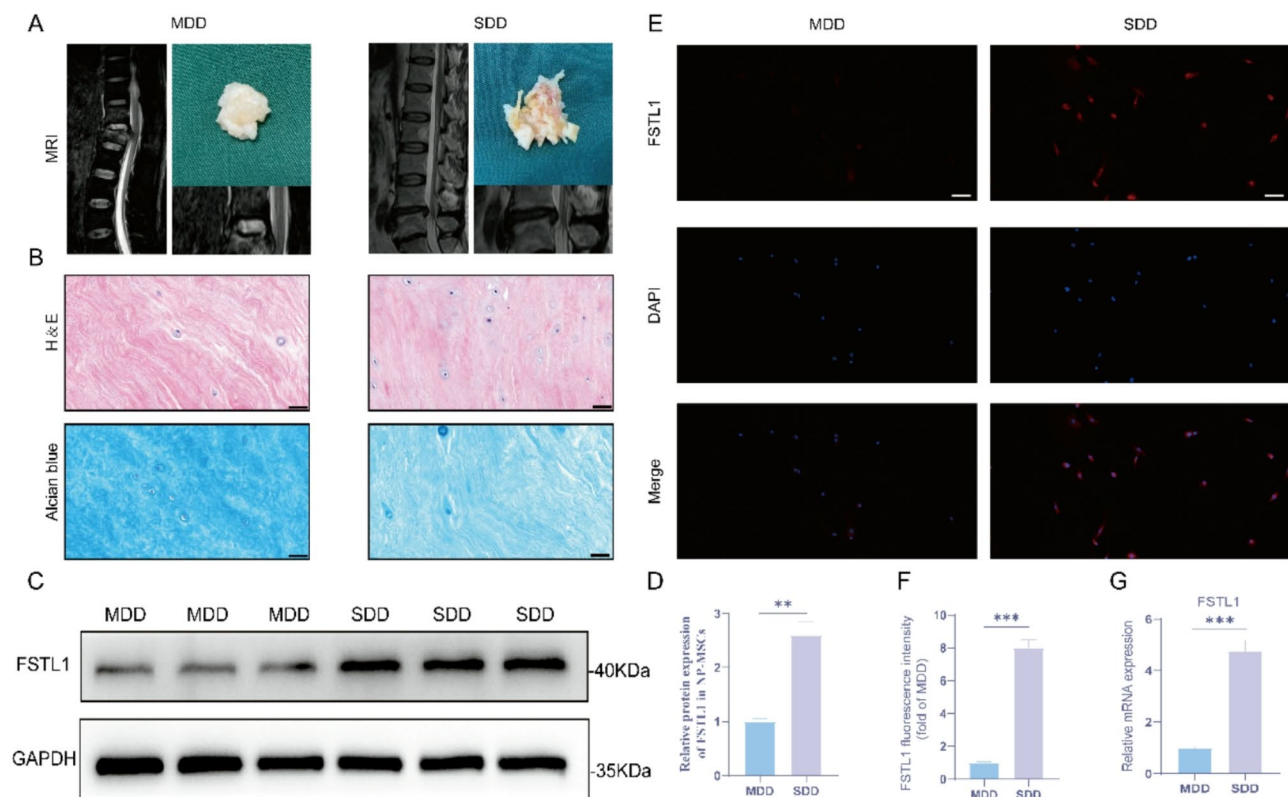


Fig. 2 FSTL1 is upregulated during disc degeneration in clinical IVDD. **(A)** Representative T2-weighted MRIs comparing mild (MDD) and severely degenerated intervertebral discs (SDD) from donors receiving IVD discectomy surgery. The gross appearance of the dissected tissues are shown in the inset. **(B)** Representative sections of NP tissue from human IVD stained with HE or Alcian blue (scale bar: 50 μ m). **(C, D)** Western blotting against FSTL1 in human NP-MSCs from MDD and SDD cases with quantitation of expression determined by Image J. **(E, F)** Representative immunofluorescence staining against FSTL1 in human NP-MSCs from MDD and SDD cases (scale bar: 50 μ m) and corresponding quantitative analysis. **(G)** RT-qPCR measurements of relative FSTL1 mRNA in NP-MSCs from MDD and SDD cases. The values are mean \pm SD for $n = 3$ determinations. * $p < 0.05$, ** $p < 0.01$, *** $p < 0.001$

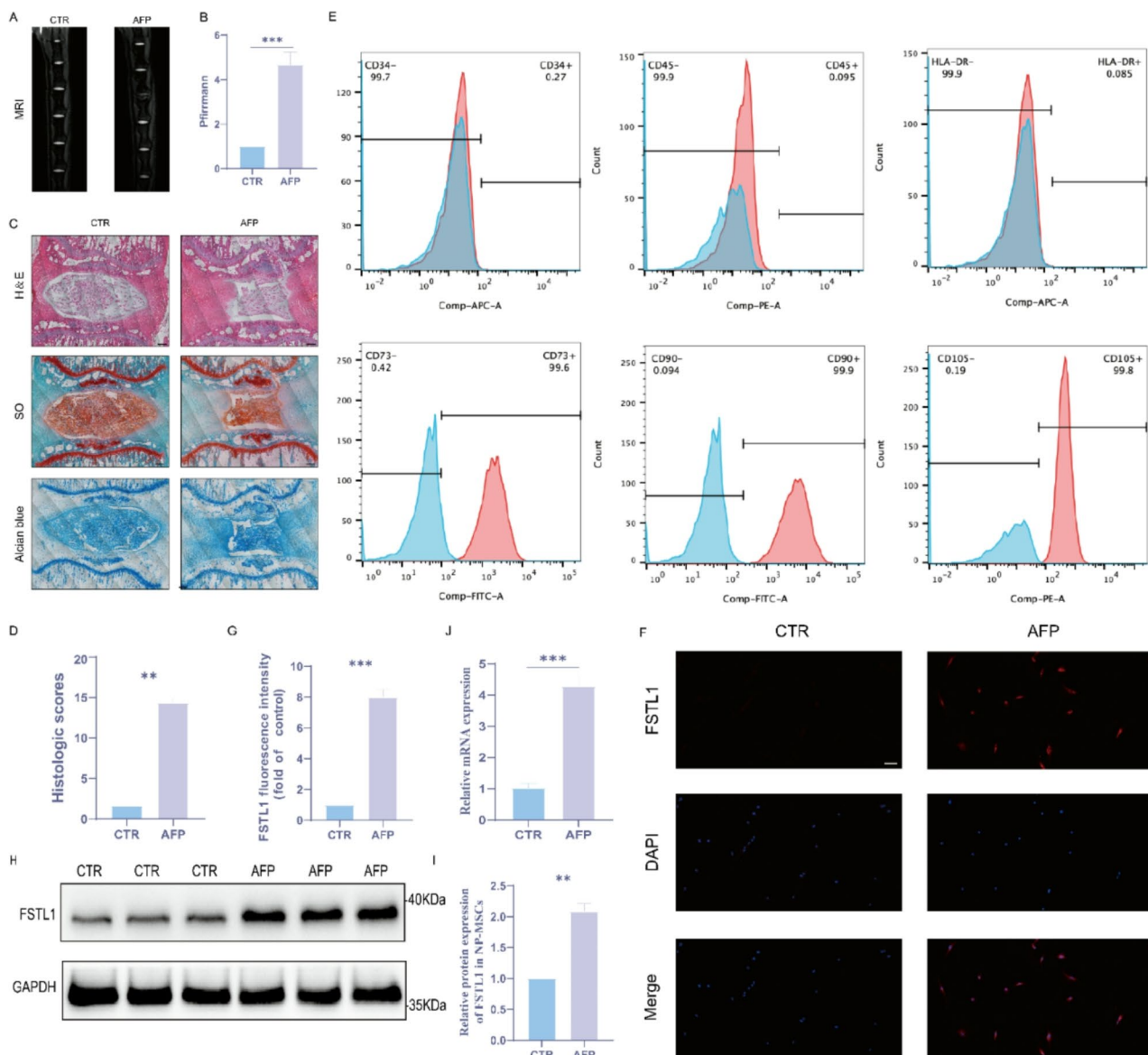


Fig. 3 FSTL1 expression is induced in NP tissues in the IVDD rat model. **(A, B)** Representative T2-weighted MRI shown for control (CTR) and annulus fibrosus punctured (AFP) rats, and quantitative comparisons of Pfirrmann grade. **(C, D)** Representative sections of NP tissues stained with HE, SO and Alcian blue (scale bar: 1 mm) and corresponding histological scores. **(E)** NP-MSCs isolated from the groups in **(A)** were subjected to flow cytometry to measure characteristic positive (CD105, CD90, CD73) and negative (CD34, CD45 and HLA-DR) markers of NP-MSCs. Representative histograms compare marker staining against an isotype control. **(F, G)** Representative immunofluorescence staining against FSTL1 in the cells from **(E)** (scale bar: 50 μ m) and corresponding quantitative analysis. **(H, I)** Western blotting against FSTL1 in the cells from **(E)** and quantitation of relative FSTL1 protein expression. **(J)** RT-qPCR measurements of relative FSTL1 mRNA in the cells from **(E)**. Values are mean \pm SD for $n=3$ determinations. * $p < 0.05$, ** $p < 0.01$, *** $p < 0.001$

CD73, CD90 and CD105 expression, and negative for CD34, CD45 and HLA-DR expression (Fig. 3E), corresponding with the known phenotype of NP-MSCs. After confirming that the cultured cells were indeed NP-MSCs, the results of immunofluorescence staining revealed a substantial increase in the quantity of FSTL1-positive cells from cultures isolated from AF puncture discs (Fig. 3F-G). Furthermore, FSTL1 mRNA and protein levels were substantially upregulated in NP-MSCs isolated from AF puncture discs (Fig. 3H-J). Therefore, the same

phenotype of increasing FSTL1 expression observed in human IVDD is evident in rat NP-MSCs, providing a foundation for exploring molecular mechanisms within the rat IVDD model.

An acidic microenvironment induces FSTL1 expression and NP-MSCs apoptosis in NP-MSCs in vitro

Our previous work established the key experimental parameters required for modelling the effects of the acidic IVD microenvironment in vitro, identifying

conditions which can inhibit NP-MSC proliferation or progressively induce apoptosis [13]. We reproduced these conditions here, subjecting NP-MSCs to a pH gradient (pH 7.0, 6.8, 6.6, 6.4) for 24 h. Western blotting assessments showed that the expression of FSTL1

was upregulated in a pH-dependent manner while the expression of apoptosis-associated markers including cleaved Caspase-3 and Bax were upregulated, while the anti-apoptotic protein Bcl-2 was downregulated (Fig. 4A-E). Analysis of further ECM related markers showed

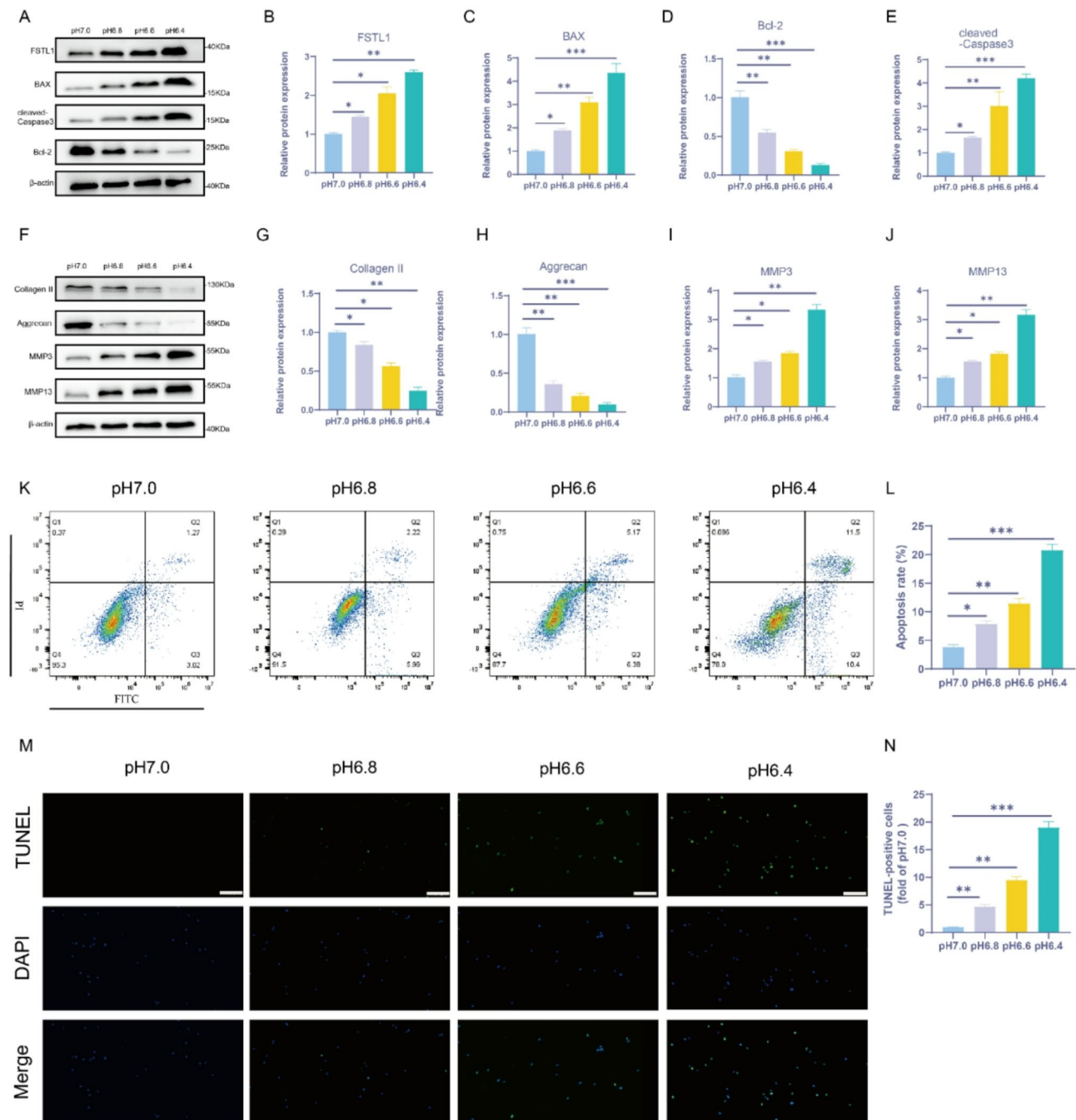


Fig. 4 pH-dependent effects on apoptosis induction in NP-MSCs. (A-E) Normal NP-MSCs were cultured under different pH conditions (pH 7.0, 6.8, 6.6, 6.4) for 24 h prior to Western blotting against FSTL1 and apoptosis-related proteins (cleaved-Caspase3, Bax, and Bcl-2) (A) and quantitative analysis of relative protein levels (B-E). (F-J) Western blotting analysis in (A) was repeated to measure changes in Collagen II, Aggrecan, MMP3, and MMP13. (K-N) The rates of apoptosis in the cells from (A) were determined using flow cytometry for Annexin V/PI staining (K, L) and TUNEL staining using epifluorescence microscopy (M, N). Representative flow dot plots (K) and quantitation (L), representative epifluorescence images (M) and quantitative analysis of TUNEL-stained cells (N) (scale bar: 100 μm). The values are mean ± SD for n = 3. *p < 0.05, **p < 0.01, ***p < 0.001

decreased ECM anabolic proteins including Collagen and Aggrecan while the catabolic proteins including MMP3 and MMP13 were upregulated (Fig. 4F-J), reflecting that acidic conditions inhibit ECM anabolism but promote ECM catabolism. Further flow cytometric assays investigating apoptosis showed a greater percentage of early apoptosis (Q3) and late apoptosis (Q2) in cultures treated with the lower pH conditions (Fig. 4K-L). These results were confirmed by TUNEL staining where the number of TUNEL-positive NP-MSCs were considerably higher in the low range pH treatments compared to milder pH-treated groups (Fig. 4M-N).

FSTL1 plays a pro-apoptotic in the acid-induced degeneration of NP-MSCs

The association between FSTL1 expression increases and apoptosis induction as revealed in the preceding section could conceivably suggest that FSTL1 plays a direct role in the acid-induced apoptosis of NP-MSCs. To address this notion, we implemented transient transfection of targeted siRNAs to silence FSTL1 expression in NP-MSCs. Notably, compared to control siRNA treatment, FSTL1 knockdown in combination with acidosis conditions at pH6.6 group resulted in significantly less TUNEL-positive NP-MSCs (Fig. 5A-B). Consistently, flow cytometric assays using dual Annexin V/PI staining showed that silencing of FSTL1 resulted in greatly reduced numbers of early apoptotic cells (Q3) and late apoptotic cells (Q2) in combination with pH6.6 treatment compared to controls (Fig. 5C-D). These results were further supported by the results of Western blotting where FSTL1 knockdown resulted in a significant decrease in the expression of acid-induced cleaved Caspase-3 and Bax proteins, while a substantial increase occurred in the expression levels of Bcl-2 (Fig. 5E-I). Together these findings suggest that FSTL1 is required to enhance apoptosis induction in NP-MSCs, at least under acidic conditions.

In addition to the aforementioned assays measuring apoptosis, we also considered how manipulating FSTL1 might affect ECM composition, a salient point given that it is a secreted protein. Indeed, following depletion of FSTL1 we observed increases in the ECM anabolic proteins Collagen and Aggrecan with decreases in the ECM catabolic proteins MMP3 and MMP13 (Fig. 5J-M). To discern more about the effects of FSTL1 on the ECM, we cultured NP-MSCs in the presence of 3 µg/mL exogenous r-FSTL1. Notably, the addition of r-FSTL1 exacerbated the degenerative effects of acidosis (pH 6.6, 24 h), causing further increases in MMP3 and MMP13 upregulation compared to acid treatment alone. Moreover, Collagen and Aggrecan expression were further downregulated in the presence of r-FSTL1 (Fig. 6A-E).

Further assessments of the impact of r-FSTL1 on NP-MSC apoptosis were also undertaken. Western blotting

results showed that r-FSTL1 addition under acid treatment conditions induced comparatively higher upregulation of cleaved Caspase-3 and Bax and downregulation of Bcl-2 expression, respectively (Fig. 6F-I). Moreover, the results of TUNEL and flow cytometry assays revealed increased numbers of apoptotic cells triggered by r-FSTL1. Furthermore, the increased number of apoptotic cells means that acid treatment successfully triggers apoptosis in NP-MSCs. Similarly, r-FSTL1 addition significantly enhances this phenotype (Fig. 6J, K). The flow cytometry confirmed the Western blotting and TUNEL labeling results, indicating a higher population of early apoptosis (Q3) and late apoptosis (Q2) in NP-MSCs treated with acid and r-FSTL1 (Fig. 6L, M).

Collectively, these results indicate that the upregulation of FSTL1 plays a direct role in the apoptosis of NP-MSCs induced by microenvironmental acidification.

FSTL1 activates TGF-β/Smad2/3 signaling in NP-MSCs

Next, we considered whether the TGF-β signaling pathway, highlighted by our RNA-seq results, was involved in pro-apoptotic actions of FSTL1 on NP-MSCs. For this, we examined if r-FSTL1 promoted changes in the expression and activity of key effectors of TGF-β signaling. Western blotting analysis revealed dose-dependent increases in Smad2 and Smad3 activation in response to r-FSTL1, as represented by the increasing ratios of phosphorylated p-Smad2/Smad2 and p-Smad3/Smad3 (Fig. 7A-C). Furthermore, in situ examination of Smad2 and Smad3 by immunofluorescence staining showed that translocation of Smad2 and Smad3 from the cytoplasm to the nucleus in NP-MSCs treated with r-FSTL1 (Fig. 7D-E). Together these data point to the likely involvement of FSTL1 in activating the TGF-β signaling pathway in NP-MSCs.

FSTL1 promotes NP-MSC apoptosis through TGF-β pathway activation

To explore the connection between FSTL1, TGF-β/Smad2/3 signaling, and acid-induced apoptosis in NP-MSCs, we incorporated SB-431542 into our experimental design, a small drug inhibitor of TGF-β receptor kinase that can suppress TGF-β pathway activity. Western blot analysis confirmed that SB-431542 significantly reversed the r-FSTL1-induced phosphorylation of Smad2 and Smad3 (Fig. 8A-C). Importantly, SB-431542 addition markedly reduced markers reflecting apoptosis with decreased expression of Caspase-3 and Bax and upregulation of Bcl-2 in acid-treated NP-MSCs (Fig. 8D-G). TUNEL staining (Fig. 8H, I) and flow cytometry (Fig. 8J, K) further demonstrated a reduction in apoptotic NP-MSCs following SB-431542 treatment. Additionally, SB-431542 counteracted the decrease in Collagen and Aggrecan expression and suppressed the upregulation

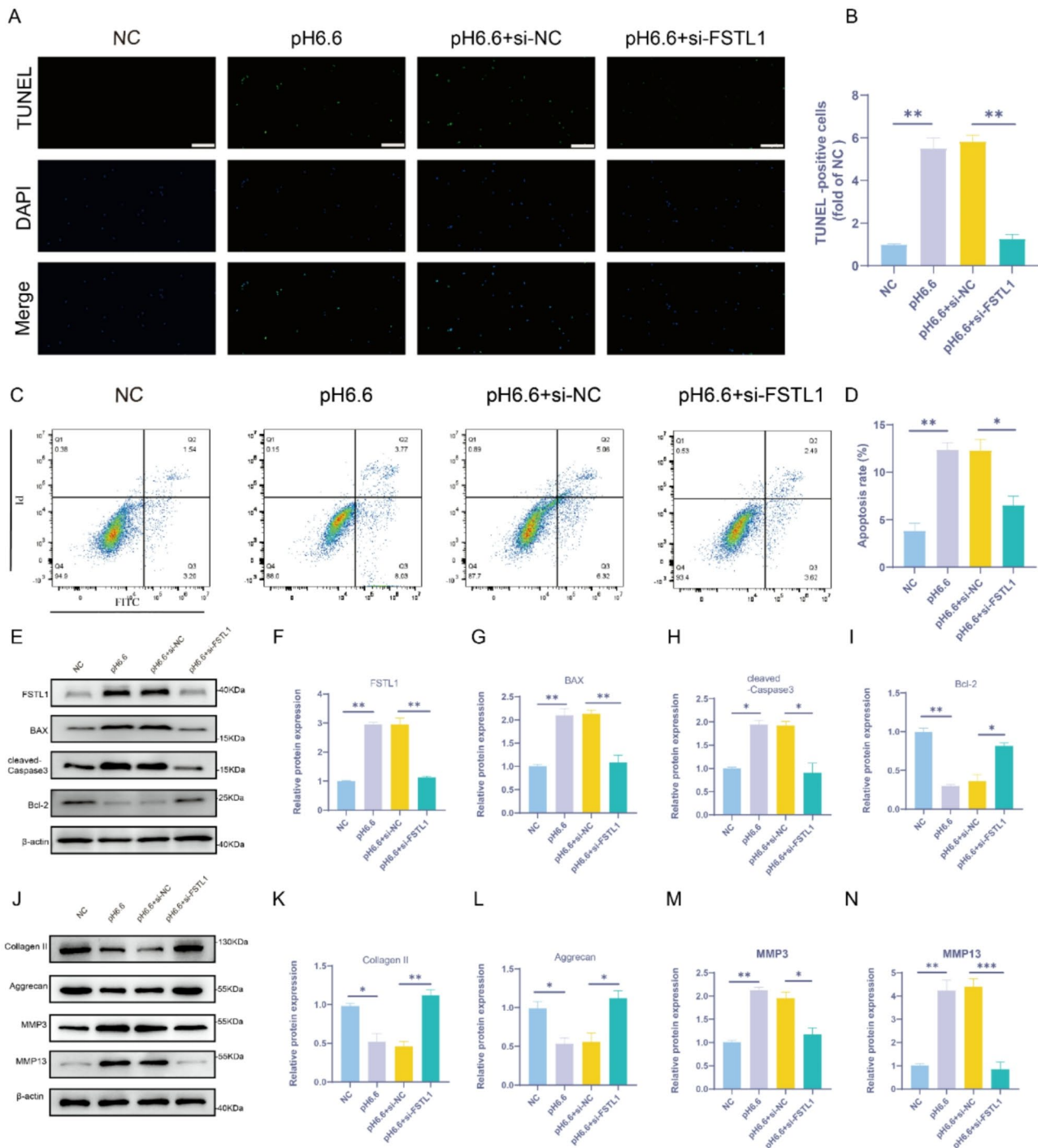


Fig. 5 Knockdown of FSTL1 using siRNA prevents acid-induced ECM degeneration and apoptosis in NP-MSCs. **(A-D)** Normal NP-MSCs exposed to control or pH 6.6 conditions or transfected with control or FSTL1 targeting siRNAs before pH 6.6 treatment were cultured for 24 h before assessing the rates of apoptosis using TUNEL assays **(A, B)** or flow cytometry measuring Annexin V/PI staining **(C, D)**. Representative epifluorescence images **(A)** and quantitative analysis of TUNEL-staining positive cells **(B)** (scale bar: 100 μm), representative flow dot plots **(C)** and quantitation **(D)**. **(E-N)** Western blotting against FSTL1 and apoptosis-related proteins (cleaved-Caspase3, Bax, and Bcl-2) **(E)** or ECM-related proteins (Collagen II, Aggrecan, MMP3, and MMP13) **(J)** with respective quantitation of protein level changes shown in **(F-I)** and **(K-N)**. The values are mean ± SD for *n* = 3. **p* < 0.05, ***p* < 0.01, ****p* < 0.001

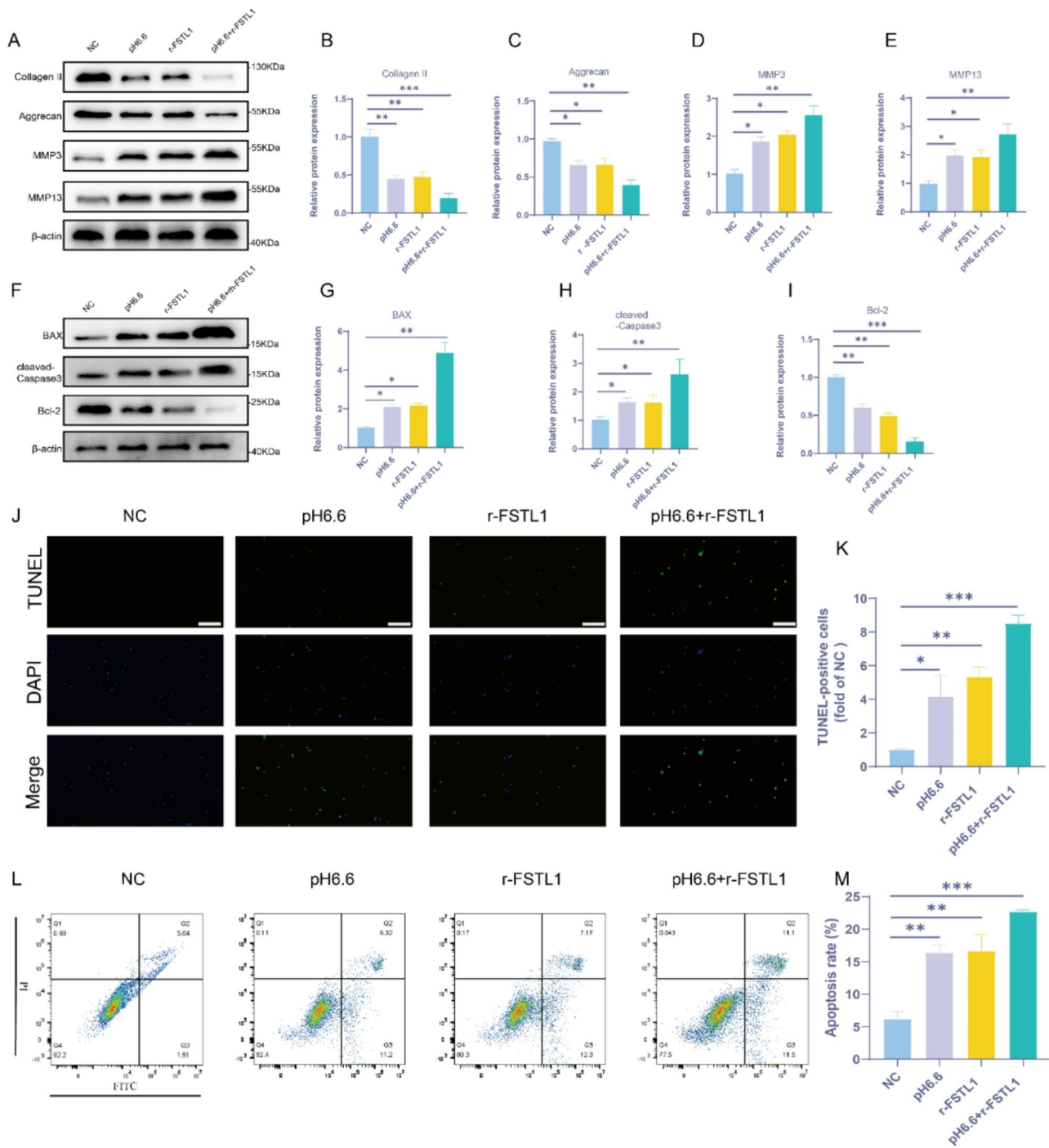


Fig. 6 Ectopic FSTL1 treatment accelerates acid-induced ECM degeneration and apoptosis in NP-MSCs. **(A-M)** Normal NP-MSCs exposed to control or pH 6.6 conditions or treated with 3 μg/mL r-FSTL1 in the presence or absence of pH 6.6 conditions were cultured for 24 h and the effects of treatment assessed using assays measuring ECM degradation **(A-E)** and apoptosis **(F-M)**, respectively. Western blotting analyses against Collagen II, Aggrecan, MMP3, and MMP13 **(A)** and quantitative analysis **(B-E)** along with blotting against the indicated apoptosis-related proteins **(F)** and accompanying quantitative analysis **(G-I)** are shown. Representative images of TUNEL staining (scale bar: 100 μm) **(J)** and quantitative analysis **(K)**, representative flow dot plots **(L)** and quantitative analysis **(M)**. The values are mean ± SD for *n* = 3 determinations. **p* < 0.05, ***p* < 0.01, ****p* < 0.001

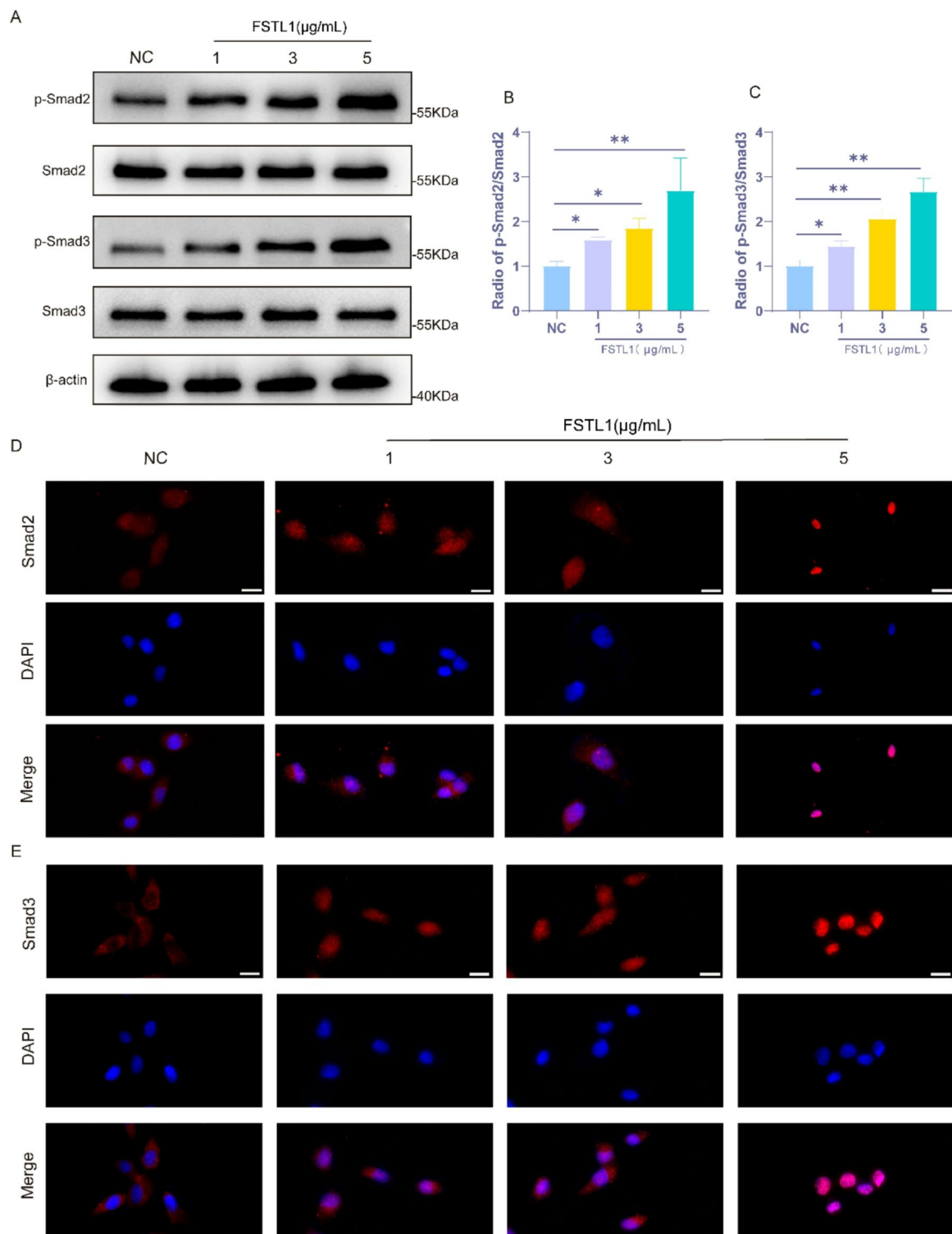


Fig. 7 Identification of TGF-β/Smad 2/3 as a target pathway of FSTL1. (A-E) Normal NP-MSCs exposed to control or treated with 1, 3, 5 μg/mL of r-FSTL1 for 24 h before assessment of the effects on Smad2 and Smad3 expression, activity and localization. Western blotting against p-Smad2, Smad2, p-Smad3 and Smad3 (A) and quantitative analysis performed to calculate the ratio of phosphorylated to total Smad levels (B, C). The cellular localization of Smad2 and Smad3 in the cells from (A) assessed by immunofluorescence staining. Representative images of Smad2 (D) and Smad3 (E) staining in combination with nuclear DAPI counterstaining (scale bar: 20 μm). The values are mean ± SD for n=3. *p < 0.05, **p < 0.01, ***p < 0.001

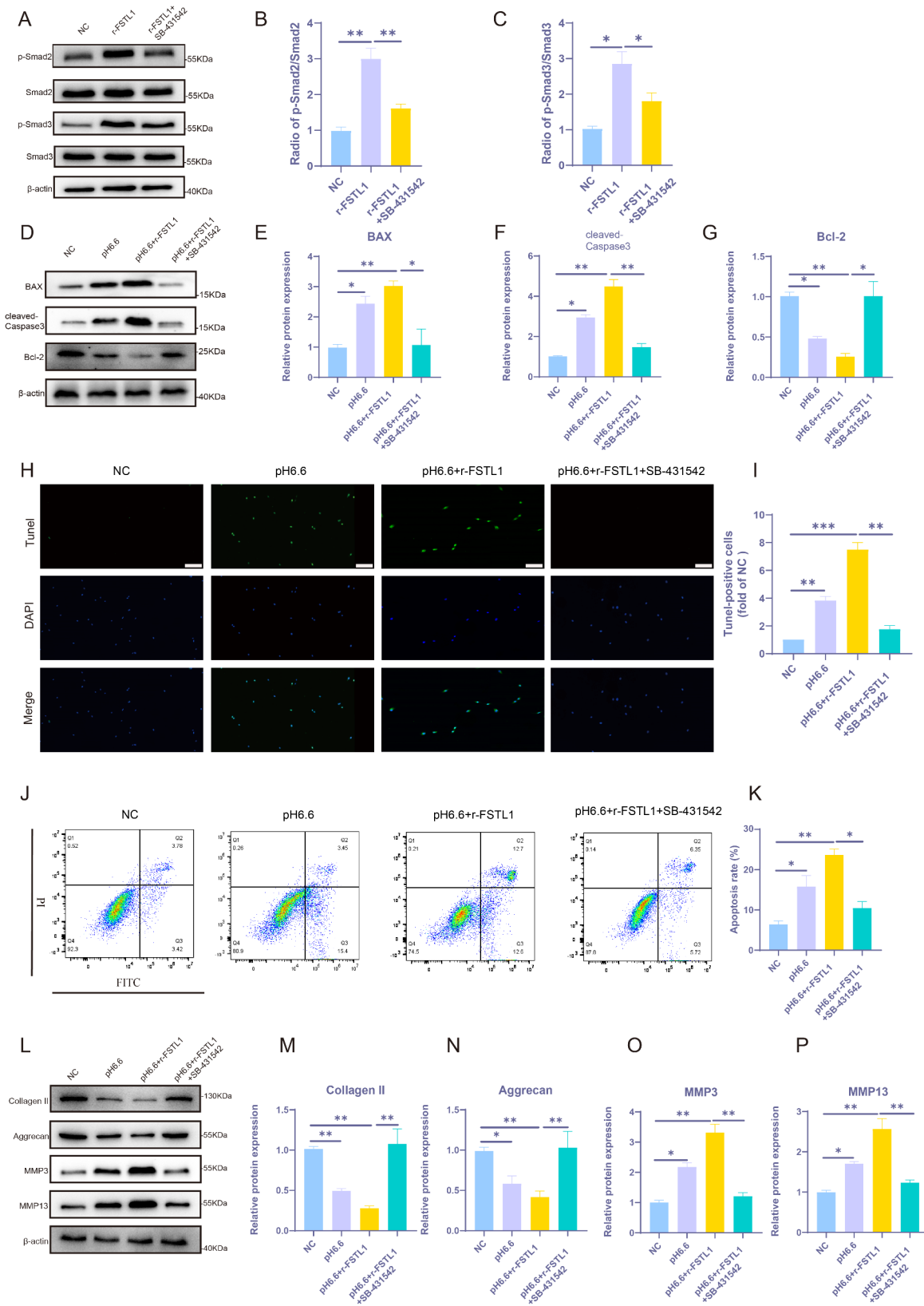


Fig. 8 (See legend on next page.)

(See figure on previous page.)

Fig. 8 FSTL1 regulates NP-MSC apoptosis and ECM degeneration by activating TGF- β -mediated Smad2/3 phosphorylation. **(A-P)** Normal untreated NP-MSCs exposed to control or treated with 3 μ g/mL r-FSTL1 in combination with 1 μ M SB-431542 (TGF- β pathway inhibitor) for 24 h before assessing the effects of treatment on TGF- β /Smad2/3 pathway activation **(A-C)**, apoptosis **(D-K)** and ECM degradative changes **(L-P)**. Western blotting against p-Smad2, Smad2, p-Smad3 and Smad3 **(A)** and quantitative analysis performed to calculate phosphorylated to total Smad ratios **(B, C)**, and changes in apoptosis-related proteins **(D)** with corresponding quantitative analyses **(E-G)**. Representative images of TUNEL staining (scale bar: 100 μ m) **(H)** and quantitative analysis **(I)**, representative flow dot plots of Annexin/PI staining **(J)** and quantitative analysis **(K)**. Western blotting analyses against Collagen II, Aggrecan, MMP3, and MMP13 **(L)** and quantitative analysis **(M-P)**. The values are mean \pm SD for $n=3$. * $p < 0.05$, ** $p < 0.01$, *** $p < 0.001$

of MMP3 and MMP13 observed in acid and r-FSTL1-treated NP-MSCs (Fig. 8L-P). Collectively, these results indicate that FSTL1 mediates NP-MSC apoptosis and ECM degradation, at least in part, through the TGF- β /Smad2/3 signaling pathway.

FSTL1 silencing in NP-MSCs ameliorates IVDD progression in the rat IVDD model

Given our findings, we reasoned that silencing FSTL1 expression in NP-MSCs could prevent their apoptotic loss following IVD transplantation and alleviate the progression of IVDD in vivo. Exploring this concept in the rat model, we sequentially injected either non-transfected NP-MSCs or those transfected with control or FSTL1 targeting siRNAs into the IVD puncture site. Four weeks following puncture and transplantation treatment, we then examined the effectiveness of this approach by conducting T2-weighted MRI scans and histological assessments. While there were no differences between the control groups (NP-MSC and NP-MSC+si-NC), we observed a significant decrease in Pfirrmann grade scores among the NP-MSC+FSTL1 siRNA group rats (Fig. 9A-B). Subsequent histological analysis of the IVD using H&E, SO, and Alcian blue staining, showed that NP-MSCs transplantation caused a delay in the reduction of NP volume and resulted in an unclear boundary between the NP and the AF, when compared to the PBS treated control group. The NP-MSC+FSTL1 siRNA group exhibited a higher number of NPCs and a more uniform ECM structure compared to the other groups. Moreover, the PBS group exhibited higher histology scores compared to all other groups, with the NP-MSC+FSTL1 siRNA group achieving lower scores compared to the NP-MSC+si-NC and NP-MSC groups (Fig. 9C-D). Thus, these experiments show that silencing FSTL1 in NP-MSCs prior to transplant provides objective benefits in vivo in delaying IVDD progression.

Discussion

While NP-MSCs hold significant promise for regenerative medicine, further progress in their therapeutic application hinges on addressing the existing challenges and limitations of this approach [36–39]. The IVDD microenvironment, characterized by hypoxia and nutrient deficiency, drives anaerobic glycolysis in NP cells, leading to acid production that diminishes NP-MSC numbers and impairs endogenous repair [4, 14, 40–42]. However, the

specific impact of this acidic environment on the viability and differentiation capacity of NP-MSCs remains poorly understood. Based on our RNA-seq analysis, we explored the role of FSTL1, a key regulator of chondrocyte growth, stem cell development, and ECM protein expression, under acidic conditions contributing to NP-MSC degeneration. Our findings demonstrated that acidification correlates with increased apoptosis in NP-MSCs, with FSTL1 exerting a pronounced pro-apoptotic effect. Mechanistically, FSTL1 facilitated apoptosis via activation of the TGF- β /Smad2/3 pathway. These results highlight the pivotal role of FSTL1 in the degenerative processes of NP-MSCs and underscore its potential impact on the development of NP-MSC-based endogenous therapies for IVDD (Fig. 10).

Through the analysis of NP-MSCs from human and rat NP tissues, we observed elevated FSTL1 expression in degenerative NP-MSCs, consistent with prior findings that FSTL1 levels increase in degenerative IVDs and NPCs [28]. Acidic conditions further amplified FSTL1 expression in a pH-dependent manner. Under these conditions, assays including TUNEL staining, Western blotting, and flow cytometry revealed heightened NP-MSC apoptosis and ECM catabolism. These outcomes align with the critical role of maintaining NP-MSC quantity and differentiation in IVD repair [43]. The acidic microenvironment inhibited NP-MSC differentiation, evidenced by reduced Collagen II and Aggrecan levels and increased MMP3 and MMP13 expression. Notably, we identified FSTL1 as a key factor accelerating NP-MSC apoptosis and ECM degradation, with FSTL1 siRNA mitigating these effects. Conversely, r-FSTL1 exacerbated these processes, increasing p-Smad2/3 expression, which was partially reversed by the SB-431542.

Building on these findings, we turned our attention to the TGF- β signaling pathway, which is widely recognized for its pivotal role in regulating tissue homeostasis, cellular proliferation, and ECM dynamics in the IVD [44–46]. Activation of TGF- β signaling has shown therapeutic promise for IVDD by enhancing ECM formation, promoting cell proliferation, and mitigating inflammation [47, 48]. However, excessive TGF- β signaling may exacerbate IVDD progression, creating a complex regulatory balance [49, 50]. Our in vitro experiments revealed that FSTL1 drives NP-MSC apoptosis and ECM degradation via activation of the TGF- β /Smad2/3 pathway. Notably, the inhibition of this pathway using SB-431542 reversed

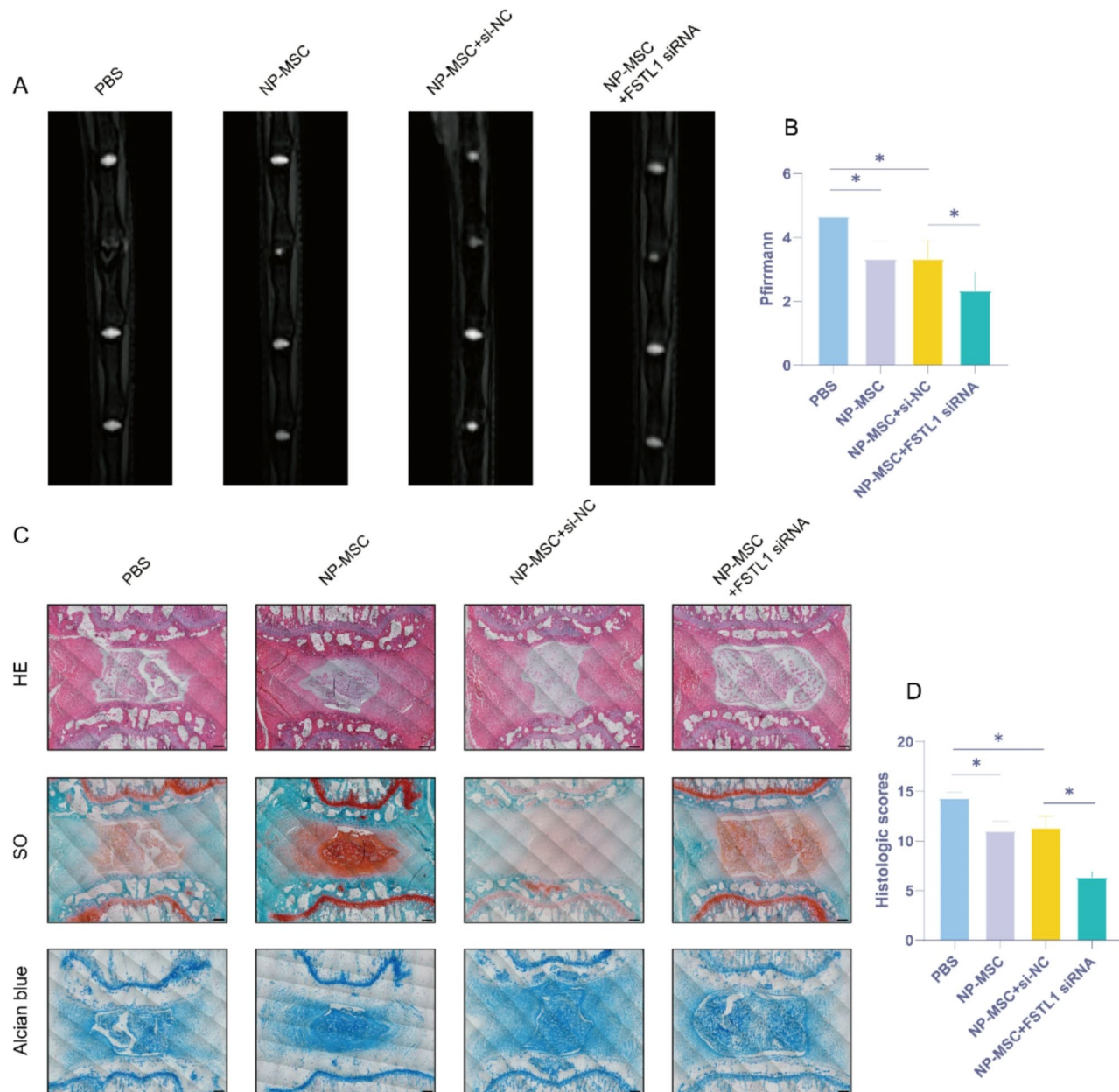


Fig. 9 FSTL1 siRNA pretreatment of NP-MSCs alleviates puncture-induced IVDD in a rat model. **(A–D)** After AF puncture, rats received mock (PBS) treatment or were transplanted twice per week (eight times in total) with untreated NP-MSCs or NP-MSCs pretreated with control siRNAs (NP-MSCs + si-NC) or FSTL1-targeting siRNAs (NP-MSCs + si-FSTL1), respectively. Representative MRI images of NP tissues comparing the different treatment groups 4 weeks after surgery **(A)** and the results of quantitative analyses based on Pfirrmann grade **(B)**. Comparative histology of the IVD among the different treatments based on HE, SO and Alcian blue staining (scale bar: 1 mm) **(C)** and histological scores **(D)**. The values are mean ± SD for $n = 3$. * $p < 0.05$, ** $p < 0.01$, *** $p < 0.001$

the effects of acid and r-FSTL1, significantly reducing NP-MSC apoptosis and ECM catabolism. These results further highlight the dualistic role of TGF- β signaling in IVD homeostasis and degeneration.

These promising *in vitro* findings were then exploited to examine if FSTL1 siRNA pretreatment could be utilized *in vivo* to enhance the differentiation and anti-apoptotic capacity of NP-MSCs. To this end, we evaluated the

therapeutic potential of FSTL1 siRNA-pretreated NP-MSCs in a rat IVDD model. Consistent with expectations, IVDs injected with these pretreated cells displayed improved water content and a stronger signal compared to control groups. Histological analyses using H&E, SO, and Alcian blue staining further corroborated the protective effects. Collectively, these results highlight the

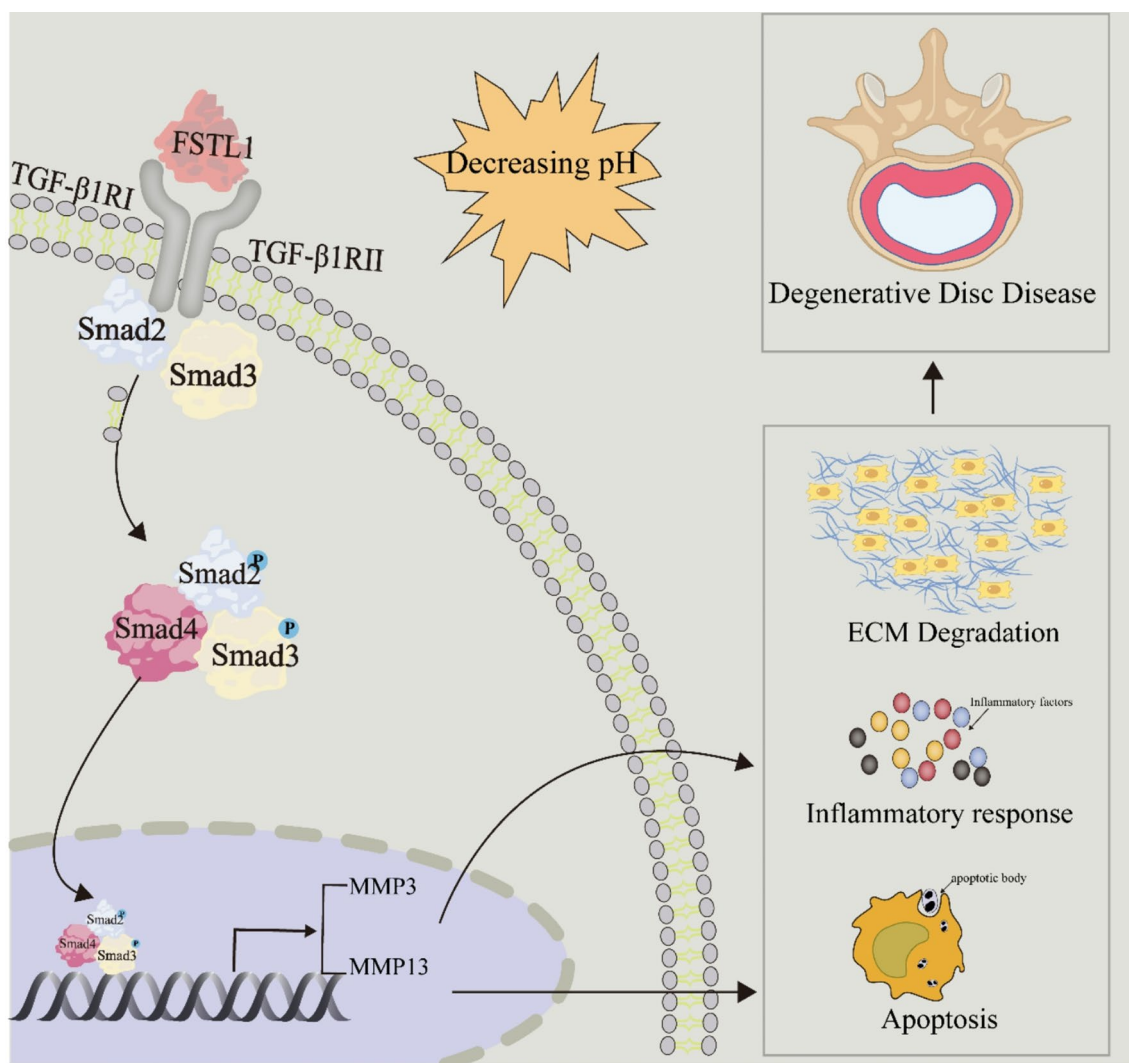


Fig. 10 Schematic model of the effects of FSTL1 in IVDD. Microenvironmental acidification induces FSTL1 expression and secretion by NP-MSCs, promoting their apoptosis through the TGF- β /Smad2/3 pathway, further facilitating ECM degradation and exacerbating inflammatory responses to promote IVDD

protective role of FSTL1 siRNA in enhancing the therapeutic efficacy of NP-MSC transplantation.

This study is not without its limitations. While we provide valuable insights into FSTL1-related processes, particularly its association with the TGF- β /Smad2/3 pathway, our RNA-seq analysis also implicates numerous other genes and pathways involved in the NP-MSC response to acidic conditions. Additionally, while our findings underscore FSTL1's role in extracellular signaling, its intracellular functions, particularly within the cytoplasm and nucleus, remain largely unexplored. Furthermore, although we demonstrated proof-of-concept efficacy in vivo, the use of genetic mouse models targeting FSTL1 expression would provide deeper insights into its role in IVDD progression. Lastly, verification in human IVDD samples will be essential to strengthen the

translational relevance of these findings and bridge the gap to clinical application.

Conclusions

In summary, our study provides the detailed insights into the mechanistic role of FSTL1 in acid-induced apoptosis of NP-MSCs and its contribution to IVDD progression. We also uncovered the function of FSTL1 within the TGF- β /Smad2/3 signaling pathway, shedding light on the molecular mechanisms essential for maintaining IVD homeostasis. Our findings reveal a novel pathway through which FSTL1 drives apoptosis and ECM degradation in NP-MSCs, positioning FSTL1 targeting as a promising therapeutic approach for IVD regeneration. These discoveries open new avenues for developing targeted interventions to address IVDD and improve regenerative medicine outcomes.

Acknowledgements

We thank Prof. Rick Thorne of Henan Provincial People's Hospital for his assistance with our manuscript.

Author contributions

XY and JYD carried out the conception and design of the research. JYD, LPZ and RJZ participated in the acquisition of data. HQZ, LK, YXW and CYJ carried out the analysis and interpretation of data. XY and JYD performed the statistical analysis. XY and RJZ drafted the manuscript, and XYL and CLS revised the manuscript. All authors read and approved the final manuscript. XY, JYD, and RJZ contributed equally to this work.

Funding

This study was supported by the National Natural Science Foundation of China (81772408, 82272551).

Data availability

We confirm that all data from this study are available within the article.

Declarations

Ethics approval and consent to participate

Studies involving human participants were reviewed and approved by the Ethics Committee of Anhui Medical University (approval No. 2017372). Animal experiments were approved and supervised by the Animal Ethics Committee of Anhui Medical University (approval No. 20170423).

Consent for publication

All the authors approved the publication.

Competing interests

The authors declare that they have no competing interests.

Author details

¹Department of Orthopedics and Spine Surgery, The First Affiliated Hospital of Anhui Medical University, 218 Jixi Road, Hefei, Anhui 230022, China

²Laboratory of Spinal and Spinal Cord Injury Regeneration and Repair, The First Affiliated Hospital of Anhui Medical University, 218 Jixi Road, Hefei, Anhui 230022, China

³Anhui Province Research Center for the Clinical Application of Digital Medical Technology, The First Affiliated Hospital of Anhui Medical University, Hefei, Anhui 230022, China

⁴School of Life Sciences, Anhui Medical University, 81 Meishan Road, Hefei, Anhui 230032, China

Received: 6 July 2024 / Accepted: 11 February 2025

Published online: 26 February 2025

References

- Hartvigsen J, Hancock MJ, Kongsted A, Louw Q, Ferreira ML, Genevay S, Hoy D, Karppinen J, Pransky G, Sieper J, et al. What low back pain is and why we need to pay attention. *Lancet*. 2018;391:2356–67.
- Global incidence, prevalence, years lived with disability (YLDs), disability-adjusted life-years (DALYs), and healthy life expectancy (HALE) for 371 diseases and injuries in 204 countries and territories and 811 subnational locations, 1990–2021: a systematic analysis for the Global Burden of Disease Study 2021. *Lancet* 2024.
- Chou D, Samartzis D, Bellabarba C, Patel A, Luk KD, Kisser JM, Skelly AC. Degenerative magnetic resonance imaging changes in patients with chronic low back pain: a systematic review. *Spine (Phila Pa 1976)*. 2011;36:S43–53.
- He R, Wang Z, Cui M, Liu S, Wu W, Chen M, Wu Y, Qu Y, Lin H, Chen S, et al. HIF1A alleviates compression-induced apoptosis of nucleus pulposus derived stem cells via upregulating autophagy. *Autophagy*. 2021;17:3338–60.
- Zhang YY, Hu ZL, Qi YH, Li HY, Chang X, Gao XX, Liu CH, Li YY, Lou JH, Zhai Y, Li CQ. Pretreatment of nucleus pulposus mesenchymal stem cells with appropriate concentration of H(2)O(2) enhances their ability to treat intervertebral disc degeneration. *Stem Cell Res Ther*. 2022;13:340.
- Ma CJ, Liu X, Che L, Liu ZH, Samartzis D, Wang HQ. Stem cell therapies for intervertebral disc degeneration: Immune Privilege reinforcement by Fas/FasL regulating Machinery. *Curr Stem Cell Res Ther*. 2015;10:285–95.
- Sakai D, Andersson GB. Stem cell therapy for intervertebral disc regeneration: obstacles and solutions. *Nat Rev Rheumatol*. 2015;11:243–56.
- Wu H, Zeng X, Yu J, Shang Y, Tu M, Cheang LH, Zhang J. Comparison of nucleus pulposus stem/progenitor cells isolated from degenerated intervertebral discs with umbilical cord derived mesenchymal stem cells. *Exp Cell Res*. 2017;361:324–32.
- Peng Y, Qing X, Lin H, Huang D, Li J, Tian S, Liu S, Lv X, Ma K, Li R, et al. Decellularized disc hydrogels for hBMSCs tissue-specific differentiation and tissue regeneration. *Bioact Mater*. 2021;6:3541–56.
- Liao Z, Luo R, Li G, Song Y, Zhan S, Zhao K, Hua W, Zhang Y, Wu X, Yang C. Exosomes from mesenchymal stem cells modulate endoplasmic reticulum stress to protect against nucleus pulposus cell death and ameliorate intervertebral disc degeneration in vivo. *Theranostics*. 2019;9:4084–100.
- Tong B, Liao Z, Liu H, Ke W, Lei C, Zhang W, Liang H, Wang H, He Y, Lei J, et al. Augmenting Intracellular Cargo Delivery of Extracellular vesicles in Hypoxic Tissues through Inhibiting Hypoxia-Induced endocytic recycling. *ACS Nano*. 2023;17:2537–53.
- Han B, Wang HC, Li H, Tao YQ, Liang CZ, Li FC, Chen G, Chen QX. Nucleus pulposus mesenchymal stem cells in acidic conditions mimicking degenerative intervertebral discs give better performance than adipose tissue-derived mesenchymal stem cells. *Cells Tissues Organs*. 2014;199:342–52.
- Liu J, Tao H, Wang H, Dong F, Zhang R, Li J, Ge P, Song P, Zhang H, Xu P, et al. Biological Behavior of Human Nucleus Pulposus Mesenchymal Stem cells in response to changes in the acidic environment during intervertebral disc degeneration. *Stem Cells Dev*. 2017;26:901–11.
- Ding J, Zhang R, Li H, Ji Q, Cheng X, Thorne RF, Hondermarck H, Liu X, Shen C. ASIC1 and ASIC3 mediate cellular senescence of human nucleus pulposus mesenchymal stem cells during intervertebral disc degeneration. *Aging*. 2021;13:10703–23.
- Sakai D, Nakamura Y, Nakai T, Mishima T, Kato S, Grad S, Alini M, Risbud MV, Chan D, Cheah KS, et al. Exhaustion of nucleus pulposus progenitor cells with ageing and degeneration of the intervertebral disc. *Nat Commun*. 2012;3:1264.
- Lyu FJ, Cheung KM, Zheng Z, Wang H, Sakai D, Leung VY. IVD progenitor cells: a new horizon for understanding disc homeostasis and repair. *Nat Rev Rheumatol*. 2019;15:102–12.
- Grunhagen T, Shirazi-Adl A, Fairbank JC, Urban JP. Intervertebral disk nutrition: a review of factors influencing concentrations of nutrients and metabolites. *Orthop Clin North Am* 2011, 42:465–477, vii.
- Jiang C, Guo Q, Jin Y, Xu JJ, Sun ZM, Zhu DC, Lin JH, Tian NF, Sun LJ, Zhang XL, Wu YS. Inhibition of EZH2 ameliorates cartilage endplate degeneration and attenuates the progression of intervertebral disc degeneration via demethylation of Sox-9. *EBioMedicine*. 2019;48:619–29.
- Xi Z, Xie Y, Sun S, Wang N, Chen S, Wang G, Li J. IVD fibrosis and disc collapse comprehensively aggravate vertebral body disuse osteoporosis and zygapophyseal joint osteoarthritis by posteriorly shifting the load transmission pattern. *Comput Biol Med*. 2024;170:108019.
- Zhang Y, Liu L, Qi Y, Lou J, Chen Y, Liu C, Li H, Chang X, Hu Z, Li Y, et al. Lactic acid promotes nucleus pulposus cell senescence and corresponding intervertebral disc degeneration via interacting with Akt. *Cell Mol Life Sci*. 2024;81:24.
- Wei K, Serpooshan V, Hurtado C, Diez-Cuñado M, Zhao M, Maruyama S, Zhu W, Fajardo G, Nosedá M, Nakamura K, et al. Epicardial FSTL1 reconstitution regenerates the adult mammalian heart. *Nature*. 2015;525:479–85.
- Guo S, Feng Y, Zhu X, Zhang X, Wang H, Wang R, Zhang Q, Li Y, Ren Y, Gao X, et al. Metabolic crosstalk between skeletal muscle cells and liver through IRF4-FSTL1 in nonalcoholic steatohepatitis. *Nat Commun*. 2023;14:6047.
- Rao J, Wang H, Ni M, Wang Z, Wang Z, Wei S, Liu M, Wang P, Qiu J, Zhang L, et al. FSTL1 promotes liver fibrosis by reprogramming macrophage function through modulating the intracellular function of PKM2. *Gut*. 2022;71:2539–50.
- Xi Y, Hao M, Liang Q, Li Y, Gong DW, Tian Z. Dynamic resistance exercise increases skeletal muscle-derived FSTL1 inducing cardiac angiogenesis via DIP2A-Smad2/3 in rats following myocardial infarction. *J Sport Health Sci*. 2021;10:594–603.
- Li X, Fang Y, Jiang D, Dong Y, Liu Y, Zhang S, Guo J, Qi C, Zhao C, Jiang F, et al. Targeting FSTL1 for multiple fibrotic and systemic Autoimmune diseases. *Mol Ther*. 2021;29:347–64.

26. Chaly Y, Blair HC, Smith SM, Bushnell DS, Marinov AD, Campfield BT, Hirsch R. Follistatin-like protein 1 regulates chondrocyte proliferation and chondrogenic differentiation of mesenchymal stem cells. *Ann Rheum Dis*. 2015;74:1467–73.
27. Li W, Alahdal M, Deng Z, Liu J, Zhao Z, Cheng X, Chen X, Li J, Yin J, Li Y, et al. Molecular functions of FSTL1 in the osteoarthritis. *Int Immunopharmacol*. 2020;83:106465.
28. Yan X, Ding JY, Zhang RJ, Zhang HQ, Kang L, Jia CY, Liu XY, Shen CL. FSTL1 Accelerates Nucleus Pulposus Cell Senescence and Intervertebral Disc Degeneration Through TLR4/NF- κ B Pathway. *Inflammation* 2024.
29. Wu M, Wu S, Chen W, Li YP. The roles and regulatory mechanisms of TGF- β and BMP signaling in bone and cartilage development, homeostasis and disease. *Cell Res*. 2024;34:101–23.
30. Cui Z, Crane J, Xie H, Jin X, Zhen G, Li C, Xie L, Wang L, Bian Q, Qiu T, et al. Halofuginone attenuates osteoarthritis by inhibition of TGF- β activity and H-type vessel formation in subchondral bone. *Ann Rheum Dis*. 2016;75:1714–21.
31. Zhu L, Yang Y, Yan Z, Zeng J, Weng F, Shi Y, Shen P, Liu L, Yang H. Controlled release of TGF- β 3 for effective local endogenous repair in IDD using rat model. *Int J Nanomed*. 2022;17:2079–96.
32. Zhen G, Wen C, Jia X, Li Y, Crane JL, Mears SC, Askin FB, Frassica FJ, Chang W, Yao J, et al. Inhibition of TGF- β signaling in mesenchymal stem cells of subchondral bone attenuates osteoarthritis. *Nat Med*. 2013;19:704–12.
33. Li X, Li L, Chang Y, Ning W, Liu X. Structural and functional study of FK domain of Fstl1. *Protein Sci*. 2019;28:1819–29.
34. Dong Y, Geng Y, Li L, Li X, Yan X, Fang Y, Li X, Dong S, Liu X, Li X, et al. Blocking follistatin-like 1 attenuates bleomycin-induced pulmonary fibrosis in mice. *J Exp Med*. 2015;212:235–52.
35. Ji ML, Jiang H, Zhang XJ, Shi PL, Li C, Wu H, Wu XT, Wang YT, Wang C, Lu J. Preclinical development of a microRNA-based therapy for intervertebral disc degeneration. *Nat Commun*. 2018;9:5051.
36. Huang ZN, Wang ZY, Cheng XF, Huang ZZ, Han YL, Cui YZ, Liu B, Tian W. Melatonin alleviates oxidative stress-induced injury to nucleus pulposus-derived mesenchymal stem cells through activating PI3K/Akt pathway. *J Orthop Translat*. 2023;43:66–84.
37. Li XC, Wang MS, Liu W, Zhong CF, Deng GB, Luo SJ, Huang CM. Co-culturing nucleus pulposus mesenchymal stem cells with notochordal cell-rich nucleus pulposus explants attenuates tumor necrosis factor- α -induced senescence. *Stem Cell Res Ther*. 2018;9:171.
38. Chen X, Zhu L, Wu G, Liang Z, Yang L, Du Z. A comparison between nucleus pulposus-derived stem cell transplantation and nucleus pulposus cell transplantation for the treatment of intervertebral disc degeneration in a rabbit model. *Int J Surg*. 2016;28:77–82.
39. Yanxia Zhu JLYLJKXGZ. MiR-146a induces the aging of mesenchymal stem cell via CASK. 2024;5:35–44. <https://doi.org/10.1007/s42764-023-00119-z>
40. Wang XB, Wang H, Long HQ, Li DY, Zheng X. LINC00641 regulates autophagy and intervertebral disc degeneration by acting as a competitive endogenous RNA of mir-153-3p under nutrition deprivation stress. *J Cell Physiol*. 2019;234:7115–27.
41. Wang J, Xia D, Lin Y, Xu W, Wu Y, Chen J, Chu J, Shen P, Weng S, Wang X, et al. Oxidative stress-induced circKIF18A downregulation impairs MCM7-mediated anti-senescence in intervertebral disc degeneration. *Exp Mol Med*. 2022;54:285–97.
42. Zhao K, An R, Xiang Q, Li G, Wang K, Song Y, Liao Z, Li S, Hua W, Feng X, et al. Acid-sensing ion channels regulate nucleus pulposus cell inflammation and pyroptosis via the NLRP3 inflammasome in intervertebral disc degeneration. *Cell Prolif*. 2021;54:e12941.
43. Sun Y, Zhang W, Li X. Induced pluripotent stem cell-derived mesenchymal stem cells deliver exogenous mir-105-5p via small extracellular vesicles to rejuvenate senescent nucleus pulposus cells and attenuate intervertebral disc degeneration. *Stem Cell Res Ther*. 2021;12:286.
44. Chen S, Lei L, Li Z, Chen F, Huang Y, Jiang G, Guo X, Zhao Z, Liu H, Wang H, et al. Grem1 accelerates nucleus pulposus cell apoptosis and intervertebral disc degeneration by inhibiting TGF- β -mediated Smad2/3 phosphorylation. *Exp Mol Med*. 2022;54:518–30.
45. Zhang Y, Li Z, Chen F, Liu H, Wang H, Li X, Liu X, Wang J, Zheng Z. TGF- β 1 suppresses CCL3/4 expression through the ERK signaling pathway and inhibits intervertebral disc degeneration and inflammation-related pain in a rat model. *Exp Mol Med*. 2017;49:e379.
46. Zheng D, Chen W, Chen T, Chen X, Liang J, Chen H, Shen H, Deng L, Ruan H, Cui W. Hydrogen ion capturing hydrogel microspheres for reversing inflammation. *Adv Mater*. 2024;36:e2306105.
47. Zhou L, Cai F, Zhu H, Xu Y, Tang J, Wang W, Li Z, Wu J, Ding Z, Xi K, et al. Immune-defensive microspheres promote regeneration of the nucleus pulposus by targeted entrapment of the inflammatory cascade during intervertebral disc degeneration. *Bioact Mater*. 2024;37:132–52.
48. Liu Y, Xue M, Han Y, Li Y, Xiao B, Wang W, Yu J, Ye X. Exosomes from M2c macrophages alleviate intervertebral disc degeneration by promoting synthesis of the extracellular matrix via MiR-124/CILP/TGF- β . *Bioeng Transl Med*. 2023;8:e10500.
49. Lu R, Xu H, Deng X, Wang Y, He Z, Xu S, Liang S, Huang X, You H, Guo F, et al. Physalin A alleviates intervertebral disc degeneration via anti-inflammatory and anti-fibrotic effects. *J Orthop Translat*. 2023;39:74–87.
50. Hu B, Xiao L, Wang C, Liu C, Zhang Y, Ding B, Gao D, Lu Y, Xu H. Circ_0022382 ameliorated intervertebral disc degeneration by regulating TGF- β 3 expression through sponge adsorption of miR-4726-5p. *Bone*. 2022;154:116185.

Publisher's note

Springer Nature remains neutral with regard to jurisdictional claims in published maps and institutional affiliations.